NANO LETTERS
Letter
Cite This: Nano Lett. 2019, 19, 7775−7780
pubs.acs.org/NanoLett

Ionic Liquid Gating Induced Protonation of Electron-Doped Cuprate Superconductors

Mohsin Rafique,[†] Zhongpei Feng,[‡,§] Zefeng Lin,[‡,§] Xinjian Wei,[‡,§] Menghan Liao,[†] Ding Zhang,*[,†,∥,⊥] Kui Jin,*[,‡,§] and Qi-Kun Xue*[,†,∥,⊥]

[†]State Key Laboratory of Low Dimensional Quantum Physics and Department of Physics, Tsinghua University, Beijing 100084, China

[‡]Beijing National Laboratory for Condensed Matter Physics, Institute of Physics, Chinese Academy of Sciences, Beijing 100190, China

[§]School of Physical Sciences, University of Chinese Academy of Sciences, Beijing 100049, China

[∥]Beijing Academy of Quantum Information Sciences, Beijing 100193, China

[⊥]Frontier Science Center for Quantum Information, Beijing 100084, China

Supporting Information

ABSTRACT: Ion injection controlled by electric field has attracted growing attention due to its tunability over bulk-like materials. Here, we achieve protonation of an electron-doped high-temperature superconductor, $La_{2-x}Ce_xCuO_4$, by gating in the electrochemical regime of the ionic liquid. Such a process induces a superconductor−insulator transition together with the crossing of the Fermi surface reconstruction point. Applying negative voltages not only can reverse the protonation process but also recovers superconductivity in samples deteriorated by moisture in the ambient. Our work extends the application of electric-field-induced protonation into high-temperature cuprate superconductors.

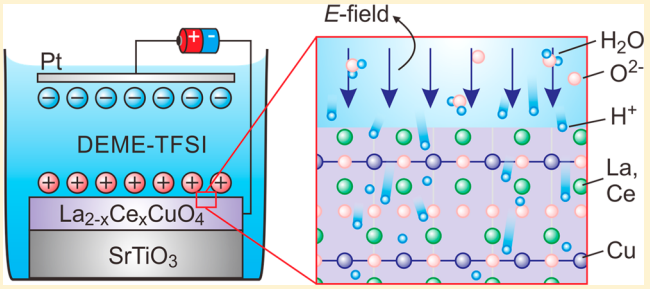

KEYWORDS: *High-temperature superconductivity, cuprate, ionic liquid, electric-double-layer transistor, protonation*

Injecting ions such as H^+, Li^+, and O^{2-} into a crystalline material may profoundly change its electrical, optical, and magnetic properties, which is of both fundamental interest and application potential.[1−7] An epitome is the metal−insulator transition realized in VO_2 by using the electric-double-layer transistor (EDLT) gating technique.[8] While the initial study suggested an electrostatic tuning,[9] subsequent studies broadened the scope by showing the involvement of electrochemical processes.[10−12] With the rapid development of EDLT, it is now possible to electrically control the migration of a variety of ions,[1] prompting further efforts in making EDLT devices for memristors, etc.[13] EDLT experiments on transition-metal oxides have demonstrated reversible tuning of both oxygen vacancies and hydrogen ions−protons. For example, a tristate switching among $SrCoO_{2.5}$, $SrCoO_3$, and a previously unknown phase, $HSrCoO_{2.5}$, was successfully realized.[2] EDLT has also proven a powerful tool in the study of high-temperature (T_c) superconductors, especially in addressing the emergence of superconductivity out of an insulating parent compound.[14] To date, such superconductor−insulator transitions (SIT) have been realized in both hole-doped cuprates of $La_{2-x}Sr_xCuO_4$,[15] $YBa_2Cu_3O_7$,[16] and $NdBa_2Cu_3O_7$[17] as well as electron-doped ones of $Pr_{2-x}Ce_xCuO_4$[17,18] and $La_{2-x}Ce_xCuO_4$ (LCCO),[19] yielding a dome-like phase diagram from the underdoped to the optimal-doped regime of a single sample. However, the electrochemical role of EDLT on the high T_c cuprate was recognized only recently. Through in operando X-ray absorption measurements, deoxygenation was identified in the liquid gated $YBa_2Cu_3O_7$.[20] Similar observation was obtained in the EDLT of $NdBa_2Cu_3O_7$.[18] On the electron-doped side, a very recent study on Pr_2CuO_4 showed that the gating mechanism can indeed cross from a purely electron-doping scheme in the positive gating[17,18,21] to the filling of oxygen vacancies in the negative gating.[22] In general, these studies focus exclusively on oxygen ions/vacancies, leaving the possible involvement of protons an open issue.

In this paper, we address just this unexplored problem. We report on the EDLT gating-induced protonation of an electron-doped cuprate superconductor, LCCO. We show that the SIT, which corresponds to the less explored doping regime from the optimal doping to the heavily overdoped side, can be reversibly achieved in samples that are even a few hundred nanometers thick. This is realized by intentionally utilizing the electrochemical window of the EDLT. The heavily

Received: July 8, 2019
Revised: October 12, 2019
Published: October 30, 2019

DOI: 10.1021/acs.nanolett.9b02776
Nano Lett. 2019, 19, 7775−7780

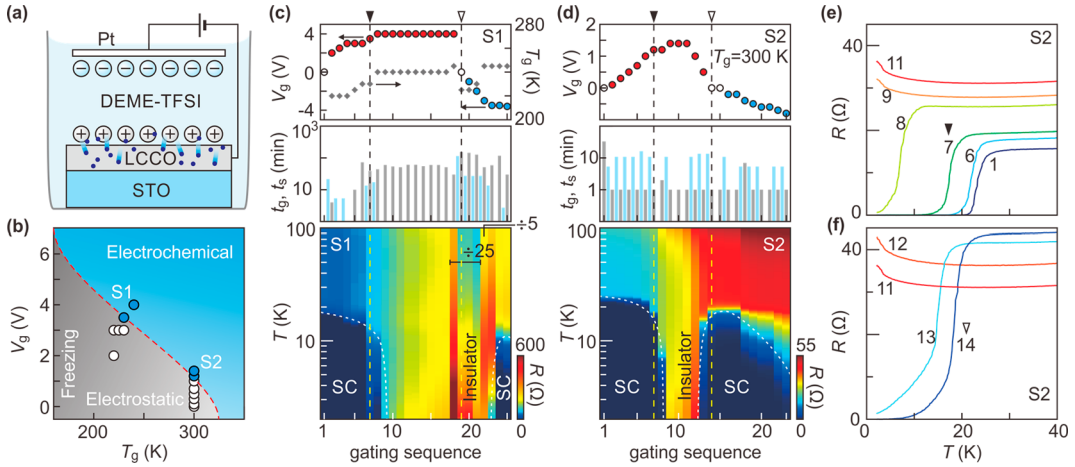

Figure 1. (a) Schematic drawing of the LCCO EDLT in the positively gated situation. Dark blue dots indicate the injection of protons, as will be explained in the main text. (b) Illustration of the operation of a LCCO EDLT in the V_g−T_g parameter space. Circles represent the gating conditions used for samples S1 and S2. Filled (empty) circles indicate that an electrochemical (electrostatic) process is involved. The dashed curve demarcates the boundary between electrostatic and electrochemical tuning. (c, d) EDLT gating conditions and the resulted temperature-dependent resistances of the two samples (S1 and S2). Gray and blue bars in the middle panels represent the gating time period and the time spent for ramping V_g (0.33−0.67 mV/s). (e, f) Temperature-dependent resistance curves of sample S2 in certain gated states. Numbers marked are gating sequences explained in panel (d).

electron-doped LCCO shows a metal−insulator transition as a function of temperature and negative magneto-resistance in the low-temperature insulating phase, suggesting enhanced scatterings when superconductivity is suppressed. The element-sensitive analysis not only reveals the reversible protonation process but also identifies the density-gradient-driven diffusion as the underlying mechanism.

Figure 1a schematically shows the EDLT fabricated on LCCO. The dominant effect of the liquid gate transits from being electrostatic at small gate voltages (V_g) and relatively lower gating temperatures (T_g) to electrochemical tuning at either large V_g or higher T_g, as indicated in Figure 1b. This phase diagram is based on the data from two samples: S1 (50 nm thick) and S2 (60 nm thick). Figure 1c,d plots the gating conditions (top panels) and the subsequent temperature-dependent resistances (bottom panels) of S1 and S2 as a function of the gating sequences. At a standard gating temperature of T_g = 220 K, which is widely used in previous gating experiments,[8] EDLT produces negligible effects up to V_g = 3 V (to the left of the vertical dashed line marked by the filled arrow in Figure 1c). This is understandable as the electric field can be easily screened[18] and the transport is dominated by the rest of such a thick sample. Further increasing V_g to 3.5 V and T_g to 230 K marks the crossover to the electrochemical regime: Sample S1 immediately shows notable change in both the resistance as well as the superconducting transition temperature (marked by the filled arrow in Figure 1c). We further settle at a gating condition of V_g = 4 V, T_g = 240 K with a timespan of about 1 h and subsequently record the resistance by cooling to 2 K and back (the last run−sequence 18 was done at 245 K with 30 min). Superconductivity gets completely suppressed after 10 such runs, reflecting bulk modulation by the electrochemical process. After this successive gating with a total gating time of about 10 h, the insulating phase becomes nonvolatile: The sample remains insulating when going back to V_g = 0 V (marked by the empty arrow in Figure 1c). Superconductivity gets recovered only when going to the negative voltages of −3.5 V, as shown in the end of the gating sequence. This hysteresis is another manifestation of the electrochemical process, as a purely electrostatic gating is volatile. The resulted superconducting transition temperature is lower than that of the initial state, and the normal state resistance becomes higher, indicating limited reversibility after the long period of gating.

A similar SIT is obtained at T_g = 300 K but at a much lower V_g and with a shorter time-span, as shown in Figure 1d. The threshold voltage for entering the electrochemical regime is reduced to 1.2−1.4 V (marked by the filled arrow in Figure 1d), which is around the standard potential of 1.23 V for the water electrolysis.[2] It suggests that H^+ ions may be created and injected into LCCO. By gating at 1.2 V with a slightly prolonged time, the superconducting transition temperature halves (sequence 7 to 8 as shown in Figure 1e). Further gating at 1.4 V results in the full suppression of superconductivity (sequence 9 as in Figure 1e). Due to the short gating time, the SIT in sample S2 is volatile, as evidenced by the step-by-step reappearance of superconductivity when going back to 0 V. Figure 1f shows that the sample resumes to show a sharp transition at around 20 K, although it is followed by a more gradual drop to zero resistance, possibly due to increased disorder. By going to more negative voltages (sequence >17 in Figure 1d), superconductivity gets suppressed again. We surmise that oxygen ions, produced previously during water electrolysis, can be pushed into the sample.[22,23] They fill the oxygen vacancies and reduce conduction carriers, which tends to drive the sample to an insulator.

The EDLT can even recover superconductivity in the deteriorated sample. Exposing LCCO samples to air for an extended period of time fully suppresses superconductivity, which is exemplified by the trace marked with 0 V in Figure 2a in a 100 nm thick sample (S3). In comparison, the sample just after growth (Figure 2b) showed superconductivity. This degradation is likely caused by the absorption of water molecules, as experience shows that storing samples in a dry cabinet or a glovebox ameliorates this problem. We fabricate an EDLT on this deteriorated sample and apply negative voltages in an attempt to withdraw these molecules. Applying V_g down to −2 V only causes an increase in resistance, which

DOI: 10.1021/acs.nanolett.9b02776
Nano Lett. 2019, 19, 7775−7780

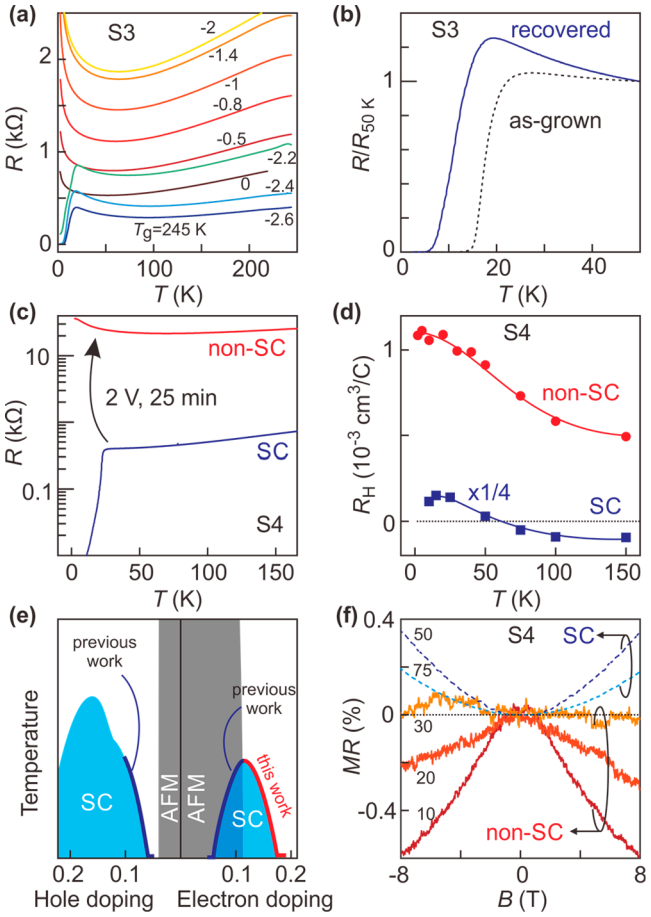

Figure 2. (a) Temperature-dependent resistances of sample S3 (100 nm thick) in the corresponding gated states (numbers represent the gating voltages). Each gating period at 245 K is around 1 h. (b) Comparison of the as-grown sample and the recovered one. The resistances are normalized by the values at 50 K. Temperature-dependent resistances (c), Hall coefficients (d), and magneto-resistances (f) of a 200 nm-thick LCCO sample (S4) before and after positive gating at 2 V, 300 K, for 25 min. (e) Phase diagrams of the electron/hole-doped cuprates with the effective doping ranges (thick curves) that can be covered by EDLT.[15−19]

may reflect the depletion of charge carriers close to the sample surface due to electrostatic gating. Slightly going below −2 V suddenly induces a drop of the normal state resistance and the emergence of superconductivity, indicating the onset of an electrochemical process that affects the bulk of the sample. Further gating gives rise to a fully superconducting sample with zero resistance at low temperatures (Figure 2b). The superconducting transition temperature is lower than that of the as-grown sample. We surmise that liquid gating breaks water molecules absorbed in LCCO into hydrogen and oxygen ions. While the hydrogen ions are extracted out of the sample, oxygen ions stay and donate holes, thus causing the sample to move from the optimal doping to the underdoped regime.

To estimate the doping level of the positively gated LCCO, we carry out magneto-transport studies. Figure 2c shows the temperature-dependent resistances of a 200 nm-thick sample (sample S4) retrieved before and after gating with 2 V for 25 min at 300 K. The temperature-dependent Hall coefficients ($R_H = d\rho_{yx}/dB$) from sample S4 before gating (Figure 2d) show the characteristic behavior[26] for LCCO close to the optimal Ce doping with a sign reversal at around 60 K. For the gated state, however, Hall measurements reveal fully positive R_H. The sample has been driven across the Fermi surface reconstruction point[24,25] (at around $x_c = 0.14$). By comparing with previous studies, the Hall coefficient and its temperature-dependent behavior reflect an equivalent Ce doping of $x > 0.18$.[25] The sample is therefore in the heavily overdoped regime, which has not been addressed before by the cuprate EDLT (summarized in Figure 2e). Electron-doped cuprates in the overdoped regime (with a high-Ce content for example) are often difficult to prepare due to structural instability. The EDLT may therefore be a powerful method to access this overdoped regime with ease. Still, the gate-induced overdoped sample shows differences than the chemically doped sample. In contrast to the Fermi-liquid metallic behavior of the overdoped LCCO with a high-Ce content,[24] a metal−insulator transition occurs in the positively gated sample (Figure 2c) with the minimum at around 65 K. The low-temperature insulating phase possesses negative magneto-resistance (*MR*), as shown in Figure 2f. Such behavior was only seen previously in the underdoped regime of LCCO and was often attributed to spin-fluctuations or localization effects.[26] The reemergence of negative *MR* in the overdoped regime by liquid gating suggests enhanced impurity scattering, presumably due to the presence of positive H^+ ions.

The difference between the liquid gate doped and the chemically doped LCCO can also be found in their structures. While the LCCO lattice contracts with an increasing Ce content (due to its smaller ionic radius than that of La), positive liquid gating causes the lattice expansion, as revealed by the X-ray diffraction (XRD). Figure 3a,b illustrates the structural change of sample S5 in the *c*-direction as a function of V_g. We ramp up V_g and obtain XRD scans (Figure 3a) in situ. Figure 3b plots the difference between the *k*-th trace and the first one. A clear shift of the LCCO (006) peak to a smaller angle, which reflects the lattice expansion, can be seen at around $V_g = 1.2$ V (indicated by the filled arrow). It gives rise to high intensities (darker region) in the color plot of Figure 3b. The lattice remains expanded even when V_g goes back to 0 V (empty arrow), suggesting a nonvolatile process. By further going to $V_g = -1$ V, the LCCO (006) peak gradually shifts back, and the intensity in Figure 3b drops. The lattice therefore shrinks.

To elucidate the electrochemical role of the LCCO EDLT, we employ the time-of-flight secondary-ion mass-spectroscopy (TOF-SIMS). Figure 3c shows the distributions of certain elements along the *z*-direction for a single sample at different gating stages: After obtaining the SIMS data for the pristine sample (left panel of Figure 3c) in an area of 100 × 100 μm^2, the same sample was gated at 1.2 V for 3 min. A second 100 × 100 μm^2 area out of the millimeter-sized sample was then investigated by SIMS, giving rise to the middle panel of Figure 3c. In the end, this sample was gated again but at −0.2 V for 30 min, and a third area was investigated by SIMS (right panel of Figure 3c). The strong signal of Cu arises from the LCCO film, whereas the $SrTiO_3$ (STO) substrate gives rise to the signal of Ti. We specifically look for the possible presence of hydrogen ions—protons. In the pristine sample, the signal of H exhibits a high intensity at the sample surface and decays rapidly into the sample, which possibly stems from hydroxide and/or hydrocarbon absorbents.[11] After the positive gating at 1.2 V, the intensity of H dramatically increases inside LCCO, whereas it remains low in the STO substrate (shaded region). Moreover, after the negative gating, the signal of H ions in LCCO

DOI: 10.1021/acs.nanolett.9b02776
Nano Lett. 2019, 19, 7775−7780

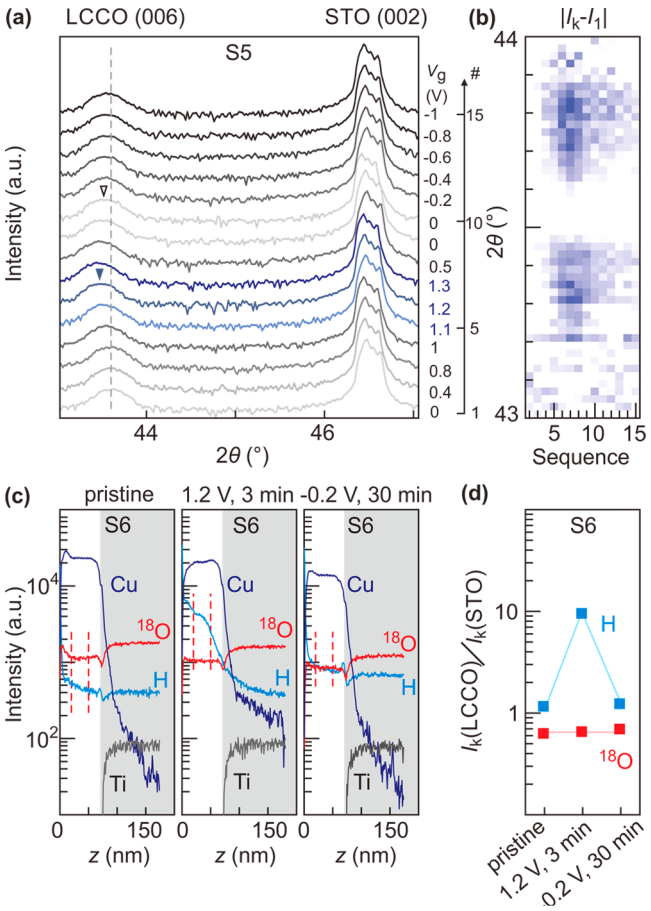

Figure 3. (a) XRD scans of sample S5 (70 nm thick) at different gating stages (denoted on the right side) at room temperature. Curves are vertically offset for clarity. Each scan was taken from $2\theta = 42°$ to 48° with a step of 0.02° in 7.5 min. When V_g reverted to 0 V, two scans were taken with a time span of about 70 min between them. (b) Color plot of the absolute difference between the XRD data of the k-th gating sequence and the first one: $|I_k - I_1|$ around the LCCO(006) peak. High intensity (darker blue) reflects large difference because of the shift of the peak position. (c) TOF-SIMS data showing the element selective intensities of a single 70 nm sample (S6) at different gating stages in sequence (left to right): pristine, gated at 1.2 V for 3 min and then gated at −0.2 V for 30 min. The signal of Cu (Ti) ions originates from the LCCO (STO) only. The depth z is estimated by taking the sputtering time where the signal of Cu drops to half of its value in LCCO as the onset of the STO substrate (shaded regions). For oxygen ions, we monitor the signal of ^{18}O because that of ^{16}O is oversaturated. (d) Normalized intensity of H ions and ^{18}O ions at different gating stages in (c). The H (^{18}O) intensity in LCCO is evaluated from the mean value in the region from z = 20 to 50 nm [indicated by the vertical dashed lines in (c)]. The H (^{18}O) intensity in the STO substrate is the mean value in the region of z > 145 nm.

decreases back to the level of that in the pristine case, attesting to the reversibility of the protonation. Figure 3d further plots the normalized intensity in the three stages. We take the average intensity of certain elements in the middle region of LCCO (indicated by the dashed lines) and normalize it by the signal of those same elements in the STO substrate. Clearly, the intensity of hydrogen increases by 1 order of magnitude in the positively gated stage and drops back after the negative gating. In contrast, the signal of oxygen (^{18}O) stays almost the same throughout the gating processes, excluding the creation of oxygen vacancies as the mechanism for the gating-induced SIT.[11] Similar results can be seen in a second sample, as shown in the Supporting Information. We conclude that liquid gating mainly causes the protonation of LCCO films.

To further understand the protonation process, we show the gating time dependence. Figure 4 shows the SIMS data with the corresponding transport results from four samples (all cut from a 10 × 10 mm^2 piece of 200 nm thick LCCO on STO). As shown in Figure 4f, the sample gated by ramping V_g to 3 V still shows a superconducting transition, although it has a lower transition temperature. By staying at 3 V with longer time spans, the samples turn fully insulating (Figure 4g,h). The protons can therefore penetrate deep into the whole film because otherwise the remnant superconductive region would still give rise to a superconducting transition in the resistance measurement. The SIMS data in Figure 4b−d clearly supports this scenario. Indeed, the signals of H at different gating stages stay almost uniform throughout the respective LCCO films, if neglecting those contributions at the interfaces. It indicates a fast diffusion process once the protons migrate to the LCCO film. We propose that this migration is driven by the large density gradient at the interface. The water electrolysis in the EDLT creates a high concentration of protons (N_0) on the top surface of LCCO, as shown in Figure 4j. The protonation rate of LCCO is proportional to the concentration difference: $\frac{dn}{dt} = C(N_0 - n)$, where C is a constant and n is the concentration of protons in LCCO. This simple model gives rise to the time dependence of n as $n(t) = N_0 - (N_0 - n_0)\exp(-Ct)$, where n_0 represents the proton concentration once V_g reaches 3 V. Figure 4k shows that the data points can be satisfactorily explained by this equation. Finally, we note that the normalized intensity of ^{18}O stays almost constant even in the case after prolonged gating (Figure 4i). We obtain similar results in a 60 nm-thick sample in the Supporting Information. It suggests that the creation of oxygen vacancies plays a negligible role in the positive gating process of LCCO thin films.

To summarize, we use EDLT on optimally doped LCCO samples and realize a SIT. Positive gating gives rise to protonation of the thick films (50−200 nm), which is driven by the large concentration gradient of protons at the interface. We show that the optimally doped LCCO with a cerium content of x = 0.1 can be protonated to the heavily overdoped regime that is equivalent to x > 0.18. Both volatile and nonvolatile states can be realized, depending on the gating conditions. The reversible control of LCCO across the Fermi surface reconstruction point may be of potential use in realizing functional devices such as oxide p−n junctions.

Methods. The c-axis oriented LCCO single crystalline films were grown on (100)-$SrTiO_3$ substrates by pulsed laser deposition technique using a KrF excimer laser.[27] The chamber was first pumped to an ultrahigh vacuum (base pressure better than 10^{-7} Torr), and then the films were deposited in an oxygen pressure of 0.1 Torr at 720−780 °C. The laser energy was set at 250−350 mJ with the frequency at 4 or 6 Hz. The films have to be annealed in situ in high vacuum to obtain optimal transition temperature. Sample thickness varies from 50 to 200 nm, that is, 40 unit cells (UC) to 160 UC. All the samples were grown with the Ce content close to the optimal doping (x = 0.10). Samples were then contacted by soldering indium. For magnetotransport measurements, a Hall bar with a width of 100 um was patterned by ion milling with a shadow mask. EDLTs were realized by immersing the sample together

DOI: 10.1021/acs.nanolett.9b02776
Nano Lett. 2019, 19, 7775−7780

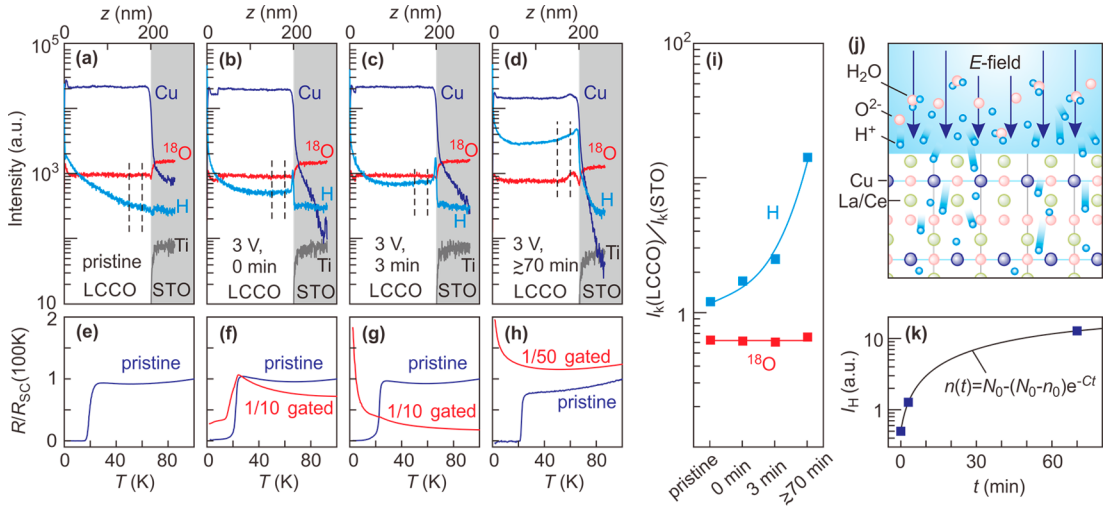

Figure 4. (a–d) Depth dependence of the element selective intensities obtained by TOF-SIMS. From left to right, the samples are (a) pristine, (b) just ramping up to 3 V, (c) gated at 3 V for 3 min, and (d) gated at 3 V for over 70 min. The gating temperature was 300 K. (e–h) Temperature-dependent resistance curves for the corresponding samples studied by SIMS in the top panels. (i) Normalized intensity of H ions and ^{18}O ions for the four samples in (a). The H (^{18}O) intensity in LCCO is evaluated from the mean value in the region from z = 150 to 180 nm (indicated by the vertical dashed lines in the top panels of (a)). The H (^{18}O) intensity in the STO substrate is the mean value in the region of z > 240 nm. (j) schematic drawing of the protonation process at the interface between the ionic liquid and the LCCO film. (k) Time dependence of the hydrogen content. Squares are data points from panel (i) after subtracting the intensity of hydrogen in the pristine sample (background level). The curve is a theoretical fit using the equation derived from a simple diffusion model.

with a Pt plate–counter electrode into the DEME-TFSI ionic liquid, as illustrated in Figure 1a. Subsequent gating and transport measurements were carried out in a physical properties measurement system equipped with a superconducting magnet (9 T). The temperature sweeps were done with a rate of 2 K/min. We employed the standard lock-in technique with an ac current of 5 μA (13 Hz) for the metallic sample and 0.5 μA for the insulating sample. For TOF-SIMS measurements, samples were bombarded by Cs^+ ions (1 keV) in a window of 100 × 100 μm^2. The XRD experiments were carried out in a Rigaku high-resolution X-ray diffractometer (9 kW) using the Cu $K_{\alpha 1}$ edge (λ=1.5406 Å).

■ ASSOCIATED CONTENT

Supporting Information

The Supporting Information is available free of charge on the ACS Publications website at DOI: 10.1021/acs.nanolett.9b02776.

Figure S1: TOF-SIMS data of a second 70 nm sample at positive/negative gating stages in sequence. Figure S2: TOF-SIMS data of three 50–60 nm-thick samples with different gating periods (PDF)

■ AUTHOR INFORMATION

Corresponding Authors

*E-mail: dingzhang@mail.tsinghua.edu.cn.
*E-mail: kuijin@iphy.ac.cn.
*E-mail: qkxue@mail.tsinghua.edu.cn.

ORCID

Ding Zhang: 0000-0002-8334-8349
Kui Jin: 0000-0003-2208-8501

Notes

The authors declare no competing financial interest.

■ ACKNOWLEDGMENTS

We acknowledge Muhammad Umair Hassan for helpful discussions. We thank Qin Zhan, Lu Yang, and Zhanping Li for technical assistance in SIMS measurements. This study was financially supported by the National Natural Science Foundation of China (11790311, 11922409, and 11604176), the Ministry of Science and Technology of China (2017YFA0302902 and 2017YFA0304600), and the Beijing Advanced Innovation Center for Future Chip (ICFC).

■ REFERENCES

(1) Leighton, C. Electrolyte-based ionic control of functional oxides. *Nat. Mater.* **2019**, *18* (1), 13–18.

(2) Lu, N.; Zhang, P.; Zhang, Q.; Qiao, R.; He, Q.; Li, H. B.; Wang, Y.; Guo, J.; Zhang, D.; Duan, Z.; Li, Z.; Wang, M.; Yang, S.; Yan, M.; Arenholz, E.; Zhou, S.; Yang, W.; Gu, L.; Nan, C. W.; Wu, J.; Tokura, Y.; Yu, P. Electric-field control of tri-state phase transformation with a selective dual-ion switch. *Nature* **2017**, *546* (7656), 124–128.

(3) Yu, Y.; Yang, F.; Lu, X. F.; Yan, Y. J.; Cho, Y.-H.; Ma, L.; Niu, X.; Kim, S.; Son, Y.-W.; Feng, D.; Li, S.; Cheong, S.-W.; Chen, X. H.; Zhang, Y. Gate-tunable phase transitions in thin flakes of 1T-TaS_2. *Nat. Nanotechnol.* **2015**, *10*, 270–276.

(4) Xiong, F.; Wang, H.; Liu, X.; Sun, J.; Brongersma, M.; Pop, E.; Cui, Y. Li Intercalation in MoS_2: In Situ Observation of Its Dynamics and Tuning Optical and Electrical Properties. *Nano Lett.* **2015**, *15* (10), 6777–84.

(5) Kuhne, M.; Paolucci, F.; Popovic, J.; Ostrovsky, P. M.; Maier, J.; Smet, J. H. Ultrafast lithium diffusion in bilayer graphene. *Nat. Nanotechnol.* **2017**, *12* (9), 895–900.

(6) Lei, B.; Wang, N. Z.; Shang, C.; Meng, F. B.; Ma, L. K.; Luo, X. G.; Wu, T.; Sun, Z.; Wang, Y.; Jiang, Z.; Mao, B. H.; Liu, Z.; Yu, Y. J.; Zhang, Y. B.; Chen, X. H. Tuning phase transitions in FeSe thin flakes by field-effect transistor with solid ion conductor as the gate dielectric. *Phys. Rev. B: Condens. Matter Mater. Phys.* **2017**, *95* (2), No. 020503.

(7) Liao, M.; Zhu, Y.; Zhang, J.; Zhong, R.; Schneeloch, J.; Gu, G.; Jiang, K.; Zhang, D.; Ma, X.; Xue, Q.-K. Superconductor–Insulator Transitions in Exfoliated $Bi_2Sr_2CaCu_2O_{8+\delta}$ Flakes. *Nano Lett.* **2018**, *18* (9), 5660–5665.

DOI: 10.1021/acs.nanolett.9b02776
Nano Lett. 2019, 19, 7775–7780

(8) Ueno, K.; Shimotani, H.; Yuan, H.; Ye, J.; Kawasaki, M.; Iwasa, Y. Field-Induced Superconductivity in Electric Double Layer Transistors. *J. Phys. Soc. Jpn.* **2014**, *83* (3), No. 032001.
(9) Nakano, M.; Shibuya, K.; Okuyama, D.; Hatano, T.; Ono, S.; Kawasaki, M.; Iwasa, Y.; Tokura, Y. Collective bulk carrier delocalization driven by electrostatic surface charge accumulation. *Nature* **2012**, *487* (7408), 459−62.
(10) Jeong, J.; Aetukuri, N.; Graf, T.; Schladt, T. D.; Samant, M. G.; Parkin, S. S. Suppression of metal-insulator transition in VO_2 by electric field-induced oxygen vacancy formation. *Science* **2013**, *339* (6126), 1402−5.
(11) Shibuya, K.; Sawa, A. Modulation of Metal-Insulator Transition in VO_2 by Electrolyte Gating-Induced Protonation. *Adv. Electron. Mater.* **2016**, *2* (2), 1500131.
(12) Passarello, D.; Altendorf, S. G.; Jeong, J.; Samant, M. G.; Parkin, S. S. Metallization of Epitaxial VO_2 Films by Ionic Liquid Gating through Initially Insulating TiO_2 Layers. *Nano Lett.* **2016**, *16* (9), 5475−81.
(13) Shi, J.; Ha, S. D.; Zhou, Y.; Schoofs, F.; Ramanathan, S. A correlated nickelate synaptic transistor. *Nat. Commun.* **2013**, *4*, 2676.
(14) Goldman, A. M. Electrostatic Gating of Ultrathin Films. *Annu. Rev. Mater. Res.* **2014**, *44* (1), 45−63.
(15) Bollinger, A. T.; Dubuis, G.; Yoon, J.; Pavuna, D.; Misewich, J.; Bozovic, I. Superconductor-insulator transition in $La_{2-x}Sr_xCuO_4$ at the pair quantum resistance. *Nature* **2011**, *472* (7344), 458−460.
(16) Leng, X.; Garcia-Barriocanal, J.; Bose, S.; Lee, Y.; Goldman, A. M. Electrostatic control of the evolution from a superconducting phase to an insulating phase in ultrathin $YBa_2Cu_3O_{7-x}$ films. *Phys. Rev. Lett.* **2011**, *107* (2), No. 027001.
(17) Zeng, S. W.; Huang, Z.; Lv, W. M.; Bao, N. N.; Gopinadhan, K.; Jian, L. K.; Herng, T. S.; Liu, Z. Q.; Zhao, Y. L.; Li, C. J.; Harsan Ma, H. J.; Yang, P.; Ding, J.; Venkatesan, T.; Ariando. Two-dimensional superconductor-insulator quantum phase transitions in an electron-doped cuprate. *Phys. Rev. B: Condens. Matter Mater. Phys.* **2015**, *92* (2), No. 020503.
(18) Zhang, L.; Zeng, S.; Yin, X.; Asmara, T. C.; Yang, P.; Han, K.; Cao, Y.; Zhou, W.; Wan, D.; Tang, C. S.; Rusydi, A.; Ariando; Venkatesan, T. The Mechanism of Electrolyte Gating on High-Tc Cuprates: The Role of Oxygen Migration and Electrostatics. *ACS Nano* **2017**, *11* (10), 9950−9956.
(19) Matsuoka, H.; Nakano, M.; Uchida, M.; Kawasaki, M.; Iwasa, Y. Signatures of charge-order correlations in transport properties of electron-doped cuprate superconductors. *Phys. Rev. B: Condens. Matter Mater. Phys.* **2018**, *98* (14), 144506.
(20) Perez-Munoz, A. M.; Schio, P.; Poloni, R.; Fernandez-Martinez, A.; Rivera-Calzada, A.; Cezar, J. C.; Salas-Colera, E.; Castro, G. R.; Kinney, J.; Leon, C.; Santamaria, J.; Garcia-Barriocanal, J.; Goldman, A. M. In operando evidence of deoxygenation in ionic liquid gating of $YBa_2Cu_3O_{7-X}$. *Proc. Natl. Acad. Sci. U. S. A.* **2017**, *114* (2), 215−220.
(21) Jin, K.; Hu, W.; Zhu, B.; Kim, D.; Yuan, J.; Sun, Y.; Xiang, T.; Fuhrer, M. S.; Takeuchi, I.; Greene, R. L. Evolution of electronic states in n-type copper oxide superconductor via electric double layer gating. *Sci. Rep.* **2016**, *6*, 26642.
(22) Wei, X.; Li, H.-b.; Zhang, Q.; Li, D.; Qin, M.; Hu, W.; He, G.; Huan, Q.; Yu, L.; Chen, Q.; Miao, J.; Yuan, J.; Zhu, B.; Kusmartseva, A.; Kusmartseva, F. V.; Silanek, A. V.; Xiang, T.; Yu, W.; Lin, Y.; Gu, L.; Yu, P.; Jin, K. Non-Volatile Superconductivity in an Insulating Copper Oxide Induced via Ionic Liquid Gating. 2019, arXiv preprint *arXiv:1906.07360*. arXiv.org e-Print archive. https://arxiv.org/abs/1906.07360, (Accessed on June 29, 2019).
(23) Zhang, D.; Ishizuka, H.; Lu, N.; Wang, Y.; Nagaosa, N.; Yu, P.; Xue, Q.-K. Anomalous Hall effect and spin fluctuations in ionic liquid gated $SrCoO_3$ thin films. *Phys. Rev. B: Condens. Matter Mater. Phys.* **2018**, *97* (18), 184433.
(24) Jin, K.; Butch, N. P.; Kirshenbaum, K.; Paglione, J.; Greene, R. L. Link between spin fluctuations and electron pairing in copper oxide superconductors. *Nature* **2011**, *476* (7358), 73−75.
(25) Sarkar, T.; Mandal, P. R.; Higgins, J. S.; Zhao, Y.; Yu, H.; Jin, K.; Greene, R. L. Fermi surface reconstruction and anomalous low-temperature resistivity in electron-doped $La_{2-x}Ce_xCuO_4$. *Phys. Rev. B: Condens. Matter Mater. Phys.* **2017**, *96* (15), 155449.
(26) Jin, K.; Zhu, B. Y.; Wu, B. X.; Vanacken, J.; Moshchalkov, V. V.; Xu, B.; Cao, L. X.; Qiu, X. G.; Zhao, B. R. Normal-state transport in electron-doped $La_{2-x}Ce_xCuO_4$ thin films in magnetic fields up to 40Tesla. *Phys. Rev. B: Condens. Matter Mater. Phys.* **2008**, *77* (17), 172503.
(27) Jin, K.; Zhang, X. H.; Bach, P.; Greene, R. L. Evidence for antiferromagnetic order in $La_{2-x}Ce_xCuO_4$ from angular magneto-resistance measurements. *Phys. Rev. B: Condens. Matter Mater. Phys.* **2009**, *80*, 012501.

DOI: 10.1021/acs.nanolett.9b02776
Nano Lett. 2019, 19, 7775−7780